Biomaterials 34 (2013) 5640–5650

Contents lists available at SciVerse ScienceDirect

Biomaterials

journal homepage: www.elsevier.com/locate/biomaterials

Glioma therapy using tumor homing and penetrating peptide-functionalized PEG–PLA nanoparticles loaded with paclitaxel

Quanyin Hu [a,1], Xiaoling Gao [b,1], Guangzhi Gu [a], Ting Kang [a], Yifan Tu [a], Zhongyang Liu [a], Qingxiang Song [b], Lei Yao [b], Zhiqing Pang [a], Xinguo Jiang [a], Hongzhuan Chen [b], Jun Chen [a,*]

[a] Key Laboratory of Smart Drug Delivery, Ministry of Education & PLA, School of Pharmacy, Fudan University, Lane 826, Zhangheng Road, Shanghai 201203, PR China

[b] Department of Pharmacology, Institute of Medical Sciences, Shanghai Jiaotong University School of Medicine, 280 South Chongqing Road, Shanghai, 200025, PR China

ARTICLE INFO

Article history:
Received 21 March 2013
Accepted 10 April 2013
Available online 29 April 2013

Keywords:
tLyp-1 peptide
Paclitaxel
Nanoparticle
Dual targeting
Chemotherapy

ABSTRACT

By taking advantage of the excessively upregulated expression of neuropilin (NRP) on the surface of both glioma cells and endothelial cells of angiogenic blood vessels, the ligand of NRP with high affinity – tLyp-1 peptide, which also contains a CendR motif ((R/K)XX(R/K)), was functionalized to the surface of PEG–PLA nanoparticles (tLyp-1-NP) to mediate its tumor homing, vascular extravasation and deep penetration into the glioma parenchyma. The tLyp-1-NP was prepared via a maleimide-thiol coupling reaction with uniformly spherical shape under TEM and particle size of 111.30 ± 15.64 nm. tLyp-1-NP exhibited enhanced cellular uptake in both human umbilical vein endothelial cells and Rat C6 glioma cells, increased cytotoxicity of the loaded PTX, and improved penetration and growth inhibition in avascular C6 glioma spheroids. Selective accumulation and deep penetration of tLyp-1-NP at the glioma site was confirmed by in vivo imaging and glioma distribution analysis. The longest survival was achieved by those mice bearing intracranial C6 glioma treated with PTX-loaded tLyp-1-NP. The findings here strongly indicate that tLyp-1 peptide-functionalized nanoparticulate DDS could significantly improve the efficacy of paclitaxel glioma therapy.

1. Introduction

Treatment for glioblastoma multiforme (GBM), a primary malignant tumor of the brain (approximately accounts for 40%), is one of the most challenging problems as no currently available treatment is curative [1,2]. Patients diagnosed with glioma have a median survival of less than 2 years [3]. Surgery remains the main treatment for glioma in which the bulk of the tumor is removed but the peripheral infiltrating part can not be completely eradicated due to the poor cellular differentiation of glioma [4]. Chemotherapy seems essential in the auxiliary treatment of glioma, while the efficiency is far from satisfaction mainly owing to the drug delivery problems, including exclusion by blood–brain barrier (BBB) and blood–brain tumor barrier (BBTB) [5,6].

As access to the brain is a considerable impediment to the application of standard chemotherapeutics for glioma, active targeting nanoparticulate drug delivery systems (DDS), especially biodegradable nanoparticles [7,8], has achieved great development in recent years with expectation of the ease of drug administration, enhancing drug accumulation at glioma site, minimizing side effects and optimizing efficacy of therapies [9,10]. Among which those DDS overcoming BBB [11], targeting glioma cells [12] or dual-targeting BBB and glioma cells [13,14] have attracted increasing interest as they show enhanced drug delivery to glioma. However, the potential disadvantage of the BBB-overcoming DDS is their non-specific distribution in the central nervous system (CNS) which could cause severe adverse effects; the drawback of the DDS targeting glioma cells is their lack of BBB-overcoming property and also remained resistant by BBTB (the formation of angiogenesis blood vessel with the gradual impairment of BBB), which also result in poor drug accumulation in glioma. The lack of precise targeting and low drug enrichment at glioma site highly limited the application of these active targeting DDS. An alternative approach to overcome these obstacles is to target the glioma vasculatures [15,16]. However, anti-angiogenic therapy has the risk of eliciting malignant progression of tumors to increase local invasion and distant metastasis [17]. Therefore, so far, tumor angiogenesis blood

* Corresponding author. Tel.: +86 21 51980066.
E-mail addresses: chenjun@fudan.edu.cn, chenjun_1974@yahoo.com.cn (J. Chen).
[1] Authors contributed equally.

0142-9612/$ – see front matter © 2013 Elsevier Ltd. All rights reserved.
http://dx.doi.org/10.1016/j.biomaterials.2013.04.025

vessels and glioma cells dual targeting represented one of the best option to improve the therapeutic efficacy of anti-glioma drug delivery and reduce unwanted side effect.

Neuropilin (NRP), a modular transmembrane protein identified as a receptor for various forms and isoforms of VEGF and members of the class 3 semaphorin family, is highly overexpressed on the surface of both glioma cells [18,19] and endothelial cells of angiogenic blood vessels [20,21], and might serve as a promising target for dual-targeting anti-glioma drug delivery. tLyp-1 peptide, a truncated form of LyP-1 with 7 amino acid (CGNKRTR), was reported as a ligand targeted to the NRP receptor with high affinity and specificity [22]. Moreover, tLyp-1 peptide contains both a tumor-homing motif and a cryptic CendR motif ((R/K)XX(R/K)) which is responsible for cell internalization and tissue penetration [23]. Here we speculated that tLyp-1 peptide could be utilized as an effective dual-targeting ligand for facilitating the tumor homing, vascular extravasation and deep penetration of a PEG–PLA nanoparticulate drug delivery system (DDS) into the glioma parenchyma (Fig. 1).

In this study, tLyp-1 peptide was functionalized to PEG–PLA nanoparticles aiming at obtaining precise dual-targeting efficacy and extensive penetration into glioma parenchyma. Using coumarin-6 as the fluorescence probe, cellular uptake of the functionalized nanoparticles and the mechanism of cellular internalization were investigated in both HUVEC cells and C6 glioma cells, the penetration ability was determined on avascular C6 glioma spheroids. Using paclitaxel (PTX) as the model drug, the efficacy of tLyp-1-functionalized nanoparticulate DDS was evaluated both in vitro and in vivo.

2. Materials and methods

2.1. Materials

Methoxypoly(ethylene glycol)$_{3000}$-poly(lactic acid)$_{34,000}$ (MePEG–PLA) and maleimide-poly(ethylene glycol)$_{3400}$-poly(lactic acid)$_{34,000}$ (Male-PEG–PLA) were kindly provided by East China University of Science and Technology. Coumarin-6, DiR (1,1′-dioctadecyl-3,3,3′,3′-tetramethyl indotricarbocyanine Iodide) and Hoechst 33258 were provided by Sigma–Aldrich (St. Louis, MO, USA). DAPI (4,6-diamidino-2-phenylindole) was purchased from Molecular Probes (Eugene, OR, USA). PTX were purchased from Xi'an Sanjiang Biological Engineering Co. Ltd (Xi'an, China), Taxol® from Bristol-Myers Squibb Company, and cell counting kit-8 (CCK-8) from Dojindo Laboratories (Kumamoto, Japan). Annexin V-FITC Apoptosis Detection kit and Apoptosis analysis Kit were purchased from Beyotime® Biotechnology Co., Ltd (Nantong, China). All other chemicals used in this study were purchased from Sinopharm Chemical Reagent Co., Ltd (Shanghai, China) unless specified otherwise.

Dulbecco's Modified Eagle's Medium (DMEM) and fetal bovine serum (FBS) were purchased from Gibco BRL (Carlsbad, CA, USA). Penicillin–streptomycin, 0.25% trypsin-EDTA and non-essential amino acid were obtained from Invitrogen Co., USA.

tLyp-1 peptide (CGNKRTR) was synthesized by ChinaPeptides Co., Ltd (Shanghai, China). Primary human umbilical vein endothelial cells (HUVEC cells) were purchased from Cascade Biologics (USA) and Rat C6 glioma cell lines were provided by Cell Institute of Chinese Academy of Sciences (Shanghai, China).

Balb/c nude mice (male, 4–5 weeks, 20 ± 2 g) were obtained from Experimental Animal Center of Fudan University and housed at 25 ± 1 °C with access to food and water ad libitum. The protocol of animal experiments was approved by the Animal Experimentation Ethics Committee of Fudan University.

2.2. Preparation of tLyp-1-NP

PEG–PLA nanoparticle loaded with PTX was prepared through the emulsion/solvent evaporation technique according to the procedure reported previously [24]. Briefly, 22.5 mg MePEG–PLA, 2.5 mg Male-PEG–PLA and 50 μg PTX were dissolved in 1 ml dichloromethane, to which 2 ml of 1% sodium cholate aqueous solution was added, and the mixture was subjected to a probe sonicator (Ningbo Scientz Biotechnology Co. Ltd., China), emulsified by sonication (280 W, 2.4 min) under ice bath. Then the emulsion formed was added into 8 ml of 0.5% sodium cholate aqueous solution under rapid magnetic stirring for 5 min. After that, the emulsion was subjected to a rotary evaporator (Shanghai Institute of Organic Chemistry, China) to remove the dichloromethane and subsequently centrifuged at 21,000g for 45 min using TJ-25 centrifuge (Beckman Counter, USA). Followed by discarding the supernatant, the obtained nanoparticles were re-suspended by 0.01 M HEPES buffer (pH 7.0) and stored at 4 °C until further use.

tLyp-1-NP was prepared via a maleimide-thiol coupling reaction at room temperature for 8 h as described previously [25]. The products were then eluted with distilled water through the 1.5 × 20 cm sepharose CL-4B column (Pharmacia Biotech, Inc., Sweden) to remove the unconjugated peptides. Coumarin-6-labeled and DiR-labeled nanoparticles were prepared with the same procedure except for containing coumarin-6 and DiR.

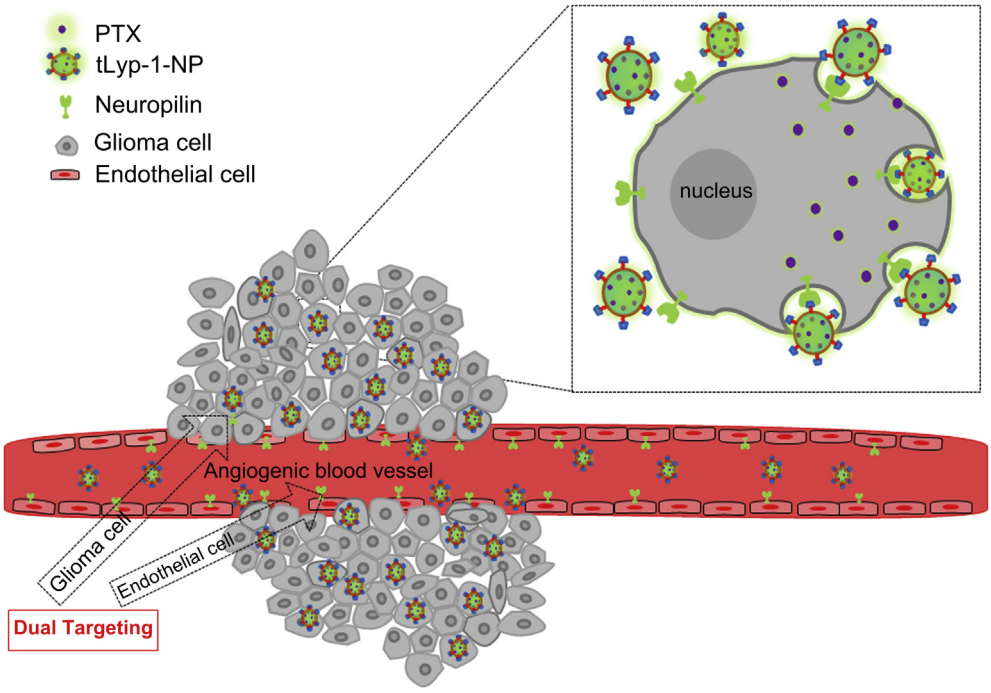

Fig. 1. Design of PTX loading tLyp-1-conjugated PEG–PLA nanoparticles as dual-targeting drug delivery system for anti-glioma therapy via NRP mediated endocytosis and penetration.

2.3. Characterization of the nanoparticles

Particle size and zeta potential of PTX-6-labeled NP (NP-PTX) and PTX-labeled tLyp-1-NP (tLyp-1-NP-PTX) were determined by dynamic light scattering detector (Zetasizer, Nano-ZS, Malvern, UK). A transmission electron microscope (TEM) (H-600, Hitachi, Japan) was used for the morphological examination of NPs following negative staining with sodium phosphotungstate solution.

To verify the conjugation of tLyp-1 peptide on the surface of NP, the NP samples were lyophilized via an ALPHA 2–4 Freeze Dryer (0.070 Mbar Vakuum, −80 °C, Martin Christ, Germany) and then subjected to X-ray photoelectron spectroscopy (XPS) analysis on a RBD upgraded PHI-5000C ESCA system (Perkin Elmer) to determine the surface composition.

2.4. Encapsulation efficiency (EE) and drug loading capacity (LC)

The encapsulation efficiency (EE) and loading capacity (LC) of PTX in NP-PTX and tLyp-1-NP-PTX were determined by high performance liquid chromatography (HPLC) as described previously [26] and calculated as indicated below ($n = 3$).

$$\mathrm{EE}(\%) = \frac{\text{PTX in the nanoparticles}}{\text{Total amount of PTX in dispersion}} \times 100\%$$

$$\mathrm{LC}(\%) = \frac{\text{Amount of PTX in nanoparticles}}{\text{nanoparticles weight}} \times 100\%$$

2.5. In vitro PTX release

In vitro PTX release from both NP and tLyp-1-NP was performed with an equilibrium dialysis method using phosphate buffer solution (PBS, pH 7.4) containing 0.5% (v/v) Tween-80 and 10% rat plasma as the release media, respectively. One milliliter freshly prepared NP and tLyp-1-NP loaded with 0.1 mg PTX were added into a dialysis bag (MWCO = 8000 Da, Greenbird Inc., Shanghai, China). Following the addition of 30 ml release medium, the mixture was incubated at 37 °C at the shaking speed of 100 rpm. Then 0.2 ml aliquots were taken out and replenished with 0.2 ml fresh release media at designed time points (1–4, 6, 8, 12, 24, 48, 72, 96 h). After that, the aliquots were subjected to HPLC analysis as described previously [27].

2.6. Cell experiments

2.6.1. Cell culture

Both HUVEC cells and C6 cells were cultured in DMEM containing 10% fetal bovine serum, 100 U/ml penicillin and 100 μg/ml streptomycin at 37 °C in a 5% CO_2/95% air humidified environment incubator (Thermo HERAcell®, USA).

2.6.2. Cellular association of the nanoparticles

Both HUVEC cells and C6 cells were seeded into 96-well plates at the density of 5×10^3 cells/well and allowed to attach for 24 h. After that, the cells were exposed to a series of concentrations of NPs loaded with coumarin-6 as fluorescence probe.

For qualitative experiment, the concentrations were ranged from 25 μg/ml to 200 μg/ml. The cells were washed twice with cold PBS buffer, fixed with 4% formaldehyde for 15 min after 1 h incubation, and then subjected to fluorescent microscopy analysis (Leica DMI4000 B, Germany).

For quantitative analysis, the cells were incubated with 200 μg/ml coumarin-6-labeled NPs for 0.5, 1–4 h, respectively. After fixation, the cells were treated with Hoechst 33258 for 15 min away from light and then subjected to a KineticScan HCS Reader (Thermo scientific, USA) for quantitative analysis. For temperature-related experiment, the plates were incubated at 37 °C, and 4 °C, respectively, at the nanoparticle concentration from 25 μg/ml to 600 μg/ml.

In order to study the mechanism of cellular uptake of tLyp-1-NP in both HUVEC cells and C6 cells, cellular association of the nanoparticles was determined in the presence of various endocytosis inhibitors including 10 μg/ml chlorpromazine, 4 μg/ml colchicines, 10 μg/ml cyto-D, 5 μg/ml BFA, 5 μg/ml filipin, 10 mM NaN_3, 50 mM deoxyglucose, 2.5 mM methyl-β-cyclodextrin (M-β-CD), 200 nM monensin, 20 μM nocodazole, and 200 μg tLyp-1 peptide. The cells were incubated in the presence of 100 μl of these inhibitors together with 100 μl 200 μg/ml coumarine-6-labeled tLyp-1-NP, respectively. The quantitative analysis was performed as described above.

2.6.3. Cell apoptosis assay

To evaluate the cell apoptosis induced by the PTX formulations, C6 glioma cells were seeded into a 6-well plate at a density of 1×10^5 cells/well. After incubation for 24 h, the cells was treated with Taxol®, NP-PTX and tLyp-1-NP-PTX (PTX concentration of 100 ng/ml), respectively, using untreated cells as the negative control. Twenty-four hours later, the cells were trypsinized, centrifuged at 1000g for 5 min, washed three times with ice-cold PBS and re-suspended in 200 ml of binding buffer. Thereafter, 5 ml of Annexin V-FITC and 10 ml of PI were added and incubated with the cells for 15 min away from light. The stained cells were analyzed using a flow cytometer (FACSCalibur, BD, USA). Data analysis was performed using Cell-Quest software (Becton Dickinson, USA).

2.6.4. Anti-proliferation assay

In vitro cytotoxicity of tLyp-1-NP on C6 cells was determined using a CCK-8 assay. Briefly, C6 cells were seeded in a 96-well plate at the density of 5×10^3 cells/well, and allowed to attach for 24 h. After that, the medium was substituted with different concentration of nanoparticles (0.001, 0.01, 0.05, 0.1, 0.8, 1 and 10 μg/ml) for 72 h. For cell viability assay, 10 μl CCK-8 was added into each well and incubated for 1 h. Then the plate was subjected to a microplate reader (Thermo Multiskan MK3, USA) for cell viability analysis at the wavelength of 450 nm.

2.7. Avascular C6 glioma spheroids experiments

2.7.1. Avascular C6 glioma spheroids formation

Avascular C6 glioma spheroids were prepared by a lipid overlay method as reported previously [28]. Briefly, a 48-well plate was initially coated with 2% (w/v) agarose gel to prevent cell adhesion. After that, C6 cells were seeded into each well at the density of 2×10^3 cells/well, gently agitated for 5 min, and incubated at 37 °C for 7 days. The uniform and compact multicellular spheroids were used for the follow-up studies.

2.7.2. Penetration in avascular C6 glioma spheroids

To evaluate the penetration ability of tLyp-1-NP, the selected spheroids were treated with 400 μg/ml NP and tLyp-1-NP loaded with coumarin-6 at 37 °C for 4 h. After that, the tumor spheroids were rinsed with cold PBS for three times, fixed with 4% formaldehyde and then subjected to laser scanning confocal microscopy analysis (LSM510, Leica, Germany).

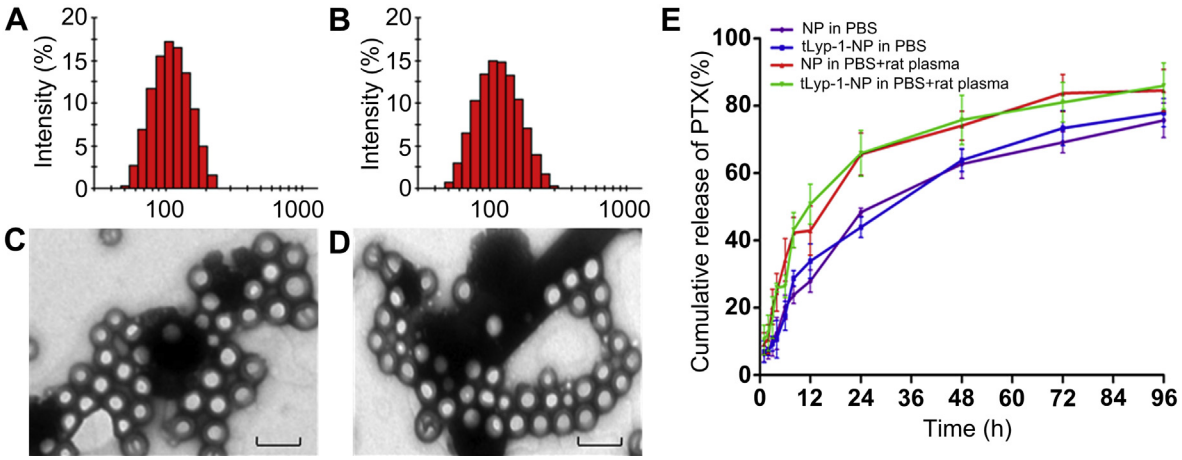

Fig. 2. Characterization of NP and tLyp-1-NP. Particle size distributions and TEM images of NP (A, C) and tLyp-1-NP (B, D). PTX release profiles from NP-PTX and tLyp-1-NP-PTX in PBS (pH 7.4) with 0.5% Tween-80 and PBS (pH 7.4) containing 10% rat plasma (C). The bar is 200 nm.

Table 1
Characterization of NP and tLyp-1-NP. Data represented mean ± SD ($n = 3$).

Nanoparticles	Particle size (nm)	Polydispersity index (PI)	Zeta potential (mV)
NP	105.32 ± 10.32	0.077 ± 0.012	−28.6 ± 4.67
tLyp-1-NP	111.30 ± 15.64	0.140 ± 0.08	−24.3 ± 3.36

2.7.3. Growth inhibition of avascular C6 glioma spheroids

For studying the growth inhibition effect of tLyp-1-NP on glioma spheroids, the spheroids (incubated for 4 days) were exposed to different PTX formulations (PTX concentration 500 ng/ml), including Taxol®, NP-PTX and tLyp-1-NP-PTX with those incubated with drug-free DMEM medium as the blank control. The growth inhibition of the avascular C6 glioma spheroids was evaluated by measuring the size of C6 glioma spheroid under an invert microscope (Chongqing Optical & Electrical Instrument, Co., Ltd., Chongqing, China) every 2 days.

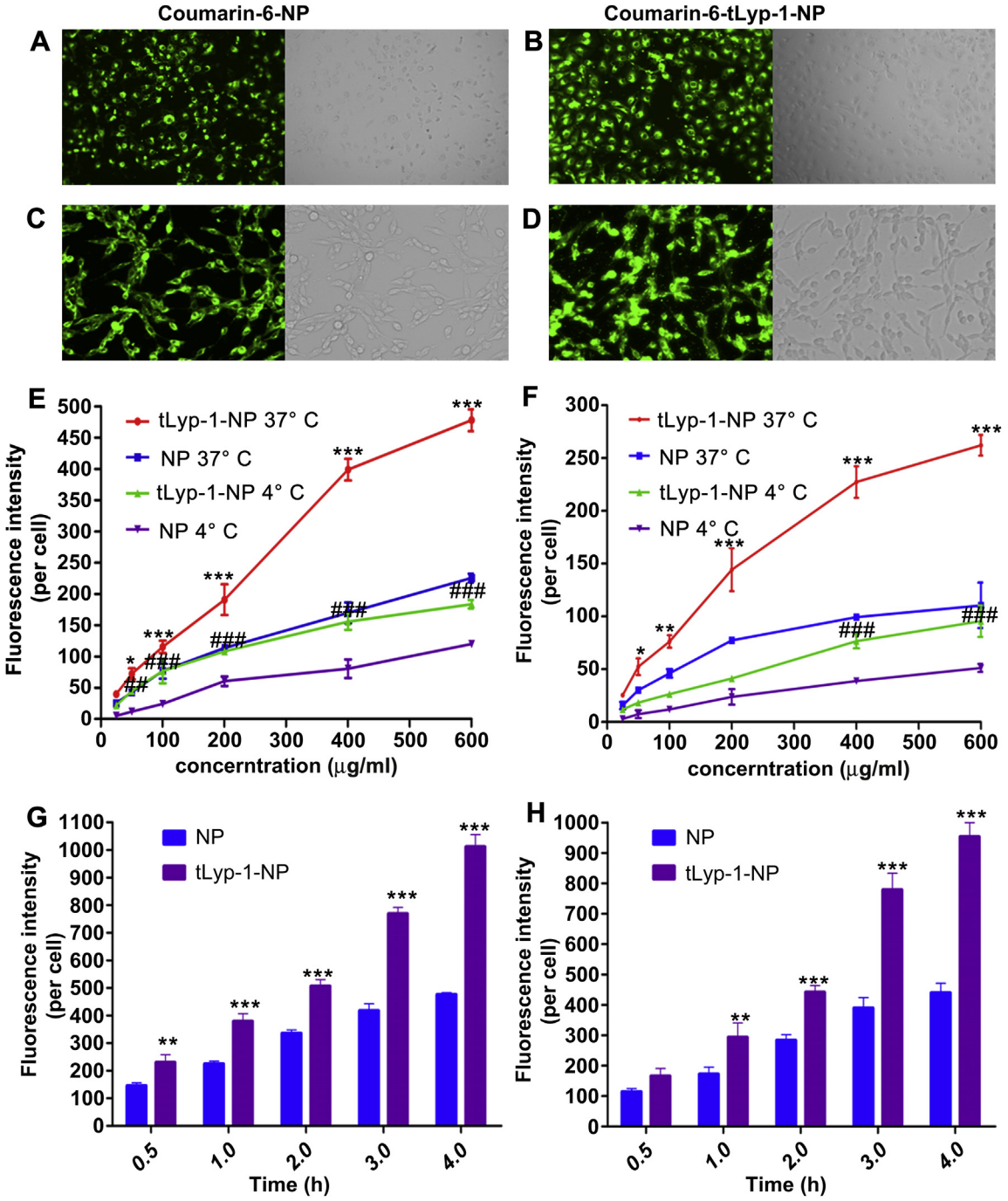

Fig. 3. Cellular association of NP and tLyp-1-NP at the nanoparticles concentration 200 μg/ml at 37 °C in HUVEC cells (A, B) and C6 cells (C, D) after 1 h incubation. Original magnification: ×20. Cellular association of coumarin-6-labeled unmodified NP and tLyp-1-NP at different temperatures (4 °C and 37 °C) after incubation for 1 h at the nanoparticle concentrations from 25 mg/ml to 600 μg/ml in HUVEC cells (E) and C6 cells (F). Cellular association of coumarin-6-labeled unmodified NP and tLyp-1-NP at different incubation time ranged from 0.5 to 4 h in HUVEC cells (G) and C6 cells (H) at nanoparticles concentration of 200 μg/ml. *$p < 0.05$, **$p < 0.01$, ***$p < 0.001$ significantly higher than the cellular uptake of unmodified NP at 37 °C, and #$p < 0.05$, ##$p < 0.01$, ###$p < 0.001$ higher than the cellular uptake of unmodified NP at 4 °C.

2.8. In vivo experiments

2.8.1. Mice model establishment

In order to reveal the performance of tLyp-1-NP in vivo, the nude mice model bearing intracranial C6 glioma was prepared by slowly injected C6 cells (5×10^5 cells/5 μl in pH 7.4 PBS) into right corpus striata of nude mice with the help of a stereotaxic apparatus. These mice were cultured under standard condition for 2 weeks and used for subsequent experiments.

2.8.2. In vivo imaging

Six nude mice bearing intracranial C6 glioma were divided into two groups randomly, and intravenously administrated with 200 μl DiR-labeled NP and tLyp-1-NP (1 mg/kg) via the tail vein. The fluorescent images were observed at predetermined time points (2, 6, 12, 24 h) via a CRi in vivo imaging system (CRi, MA, USA). Twenty-four hours after administration, the mice were sacrificed with the brains and other organs harvested and imaged.

2.8.3. Glioma distribution

Nude mice bearing intracranial C6 glioma ($n = 3$) were intravenously administered with coumarin-6-loaded NP and tLyp-1-NP, respectively, at the equal dose of coumarin-6. Three hours later, the mice were anesthetized, and heart perfused with saline and 4% paraformaldehyde. Then the brains were collected, fixed in 4% paraformaldehyde and then dehydrated in 10%, 30% sucrose solution. Afterward, the brains were imbedded in OCT (Sakura, Torrance, CA, USA), frozen at −80 °C and sectioned at 10 μm. Finally, the slides were subjected to confocal microscopy analysis (LSM710, Leica, Germany) after stained with DAPI for 10 min and rinsed with PBS.

2.8.4. Anti-glioma effect

Twenty-four nude mice bearing intracranial C6 glioma were divided into four groups randomly ($n = 6$), intravenously administered with Taxol®, NP-PTX and tLyp-1-NP-PTX (PTX concentration of 5 mg/kg) and saline, respectively, every three days in two weeks. The survival time of each group was recorded and analyzed.

2.9. Statistical analysis

All the data were presented as mean ± standard deviation. Unpaired student's *t* test was used for between two-group comparison and one-way ANOVA with Bonferroni tests for multiple-group analysis. Statistical significance was defined as $p < 0.05$.

3. Results

3.1. Characterization of the nanoparticles

The particle sizes of NP and tLyp-1-NP were 105.32 ± 10.32 nm and 111.30 ± 15.64 nm, respectively. The polydispersity index, zeta potential and size distribution were shown in Fig. 2A and B and Table 1. NP and tLyp-1-NP exhibited the same spherical shape under TEM (Fig. 2C and D). Encapsulation of PTX, coumarin-6 and DiR did not significantly change the particle size.

The existence of tLyp-1 peptide on the surface of nanoparticles was confirmed by XPS analysis with 0.53% nitrogen on the surface of tLyp-1-NP but undetectable on that of NP.

The LC of NP and tLyp-1-NP was 1.65 ± 0.07% and 1.43 ± 0.10%, respectively, with the EE 49.6 ± 3.2% and 47.5 ± 2.4%, respectively.

3.2. In vitro PTX release

NP-PTX and tLyp-1-NP-PTX presented almost the same release behavior, achieving cumulative PTX release 75.67 ± 5.1% and 77.91 ± 4.2%, respectively, after 96 h incubation in PBS (pH 7.4). A faster release pattern was obtained for both NP-PTX and tLyp-1-NP-PTX in PBS (pH 7.4) containing 10% rat plasma (84.50 ± 6.2% for NP-PTX, 85.86 ± 6.8% for tLyp-1-NP-PTX, respectively, after 96 h incubation) (Fig. 2E).

3.3. Cell experiments

3.3.1. Cellular association of the nanoparticles

Coumarin-6 was used as the fluorescent probe to study the cellular uptake characteristics of tLyp-1-NP. Qualitative fluorescent images showed that both HUVEC cells and C6 cells treated with tLyp-1-NP exhibited much higher fluorescence intensity than that treated with unmodified NP at the same nanoparticle concentration (200 μg/ml) (Fig. 3A–D).

Quantitatively, cellular association of coumarin-6-labeled tLyp-1-NP in both HUVEC and C6 cells displayed a concentration- and time-dependent behavior. The cellular associated fluorescence intensity of tLyp-1-NP in both cells was significantly higher than that of unmodified NP at the concentrations ranged from 25 μg/ml to 600 μg/ml and after the incubation time ranged from 0.5 h to 4 h (Fig. 3E–H). When compared with that of unmodified NP, the cellular uptake of tLyp-1-NP was 2.12, 2.37 folds higher at nanoparticles concentration of 600 μg/ml at 37 °C and 2.13, 2.17 folds higher at 4 h in HUVEC and C6 cells, respectively. In addition, both tLyp-1-NP and NP exhibited much higher cellular associations at 37 °C than 4 °C in both cells.

In HUVEC, cellular association mechanism assay showed that the uptake of tLyp-1-NP was restricted by BFA ($p < 0.01$), filipin ($p < 0.001$), NaN_3 + dg ($p < 0.001$), M-β-CD ($p < 0.001$), monensin ($p < 0.001$), nocodazole ($p < 0.001$) when compared with the non-inhibited control (Fig. 4A). Additionally, pre-addition of 200 μg tLyp-1 peptides significantly inhibited the uptake of tLyp-1-NP.

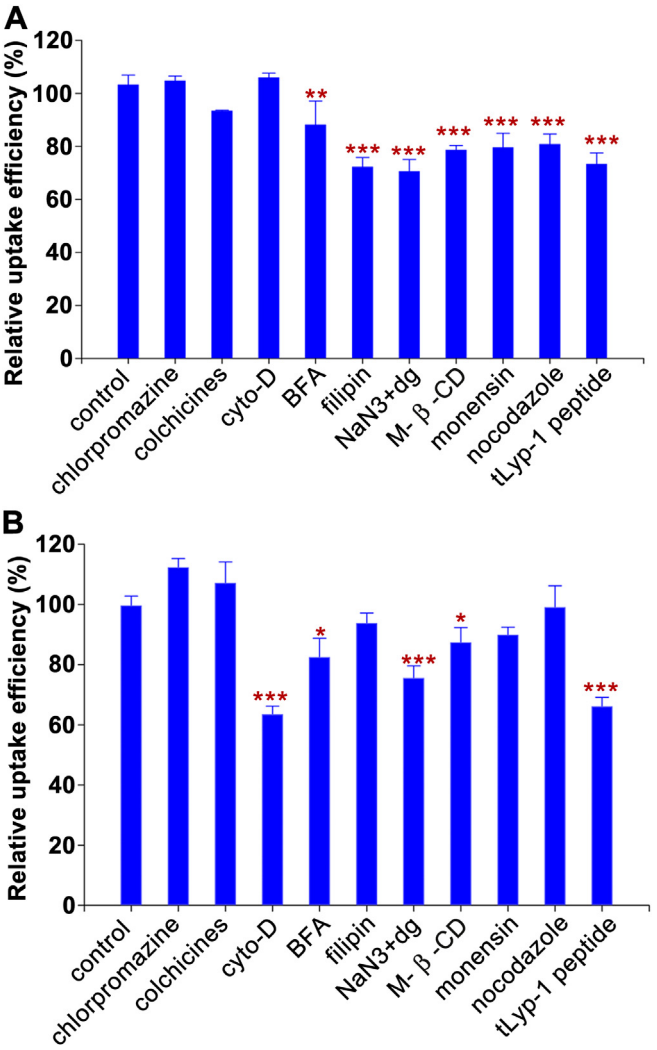

Fig. 4. Cellular association of coumarin-6-labeled tLyp-1-NP in the presence of different endocytosis inhibitors in HUVEC cells (A) and C6 cells (B). Fluorescence intensity in the non-inhibited cells, representing the maximum internalized amount of coumarin-6-labeled tLyp-1-NP, was taken as control. Data represented mean ± SD ($n = 3$). *$p < 0.05$, **$p < 0.01$, ***$p < 0.001$ significantly different with that of control.

In contrast, in C6 cell, incubation with cyto-D, BFA, NaN_3 + dg and M-β-CD significantly decreased the internalization of tLyp-1-NP by 63.5% ($p < 0.001$), 82.5% ($p < 0.05$), 75.5% ($p < 0.001$) and 85.8% ($p < 0.05$), respectively. Similarly, pre-incubation with 200 μg tLyp-1 peptides reduced the uptake of tLyp-1-NP by 66.3% ($p < 0.001$).

3.3.2. Cell apoptosis assay

C6 glioma cells were used to study cell apoptosis induced by various PTX formulations. As shown in Fig. 5A, the nuclei of untreated C6 cells showed no evidence of segmentation and fragmentation after Hoechst 33258 staining. In contrast, unsharp borders and fragmentation were observed in C6 cells treated with the PTX formulations, among which the nuclei of C6 cells exposed to tLyp-1-NP-PTX became severely fragmented.

Quantitative flow cytometry data showed that the percentage of early and late apoptosis of untreated C6 cells was 2.53 ± 0.45% and 0.87 ± 0.11%, respectively. After treated with the PTX formulations for 24 h, the percentage of early and late apoptosis was enhanced to 7.03 ± 1.67%, 2.18 ± 0.87% for Taxol®, 7.38 ± 1.35%, 1.47 ± 0.69% for NP-PTX, and 17.76 ± 3.32%, 2.84 ± 1.01% for tLyp-1-NP-PTX, respectively.

3.3.3. Anti-proliferation assay

The anti-proliferative effect of Taxol®, NP-PTX and tLyp-1-NP-PTX on C6 cells was evaluated using CCK-8 method. As shown in Fig. 6, the tLyp-1-NP-PTX formulations showed the highest anti-proliferation ability with IC_{50} 0.087 μg/ml, while that for NP-PTX and Taxol® were 0.22 μg/ml and 0.31 μg/ml, respectively.

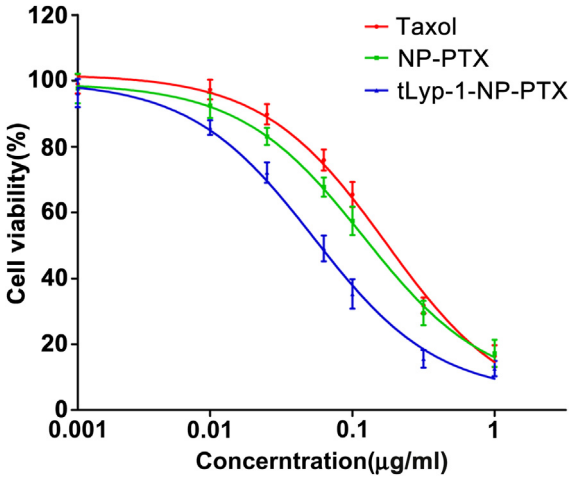

Fig. 6. Cell viability of C6 cells after treatment with Taxol®, NP-PTX and tLyp-1-NP-PTX for 72 h at 37 °C.

3.4. Avascular C6 glioma spheroids experiments

3.4.1. Penetration in avascular C6 glioma spheroids

Penetration experiment in avascular C6 glioma spheroids was performed to determine the penetrating efficacy of tLyp-1-NP. As shown by confocal microscopy analysis, tLyp-1-NP penetrated deeper and distributed more extensive in the C6 glioma spheroids than NP (Fig. 7A and C). The penetrating depth of tLyp-1-NP was 1.32 folds deeper than that of NP (121.69 μm for tLyp-1-NP, 92.02 μm for NP) (Fig. 7B and D).

3.4.2. Growth inhibition to avascular C6 glioma spheroids

In order to evaluate the inhibitory effect of different PTX formulations on tumor growth, avascular C6 glioma spheroids were treated with serum-free DMEM, Taxol®, NP-PTX and tLyp-1-NP-PTX, respectively. As shown in Fig. 8, the size of C6 glioma spheroids at the end of the experiment (Day 12) followed the order: drug-free control > Taxol® > NP-PTX > tLyp-1-NP-PTX. The glioma spheroids exposed to DMEM continued to grow along the experimental period and became tightly organized (Fig. 8A), while those incubated with tLyp-1-NP-PTX became distorted with many cells dissociated from sphere and the growth of the whole spheroids significantly inhibited (Fig. 8D).

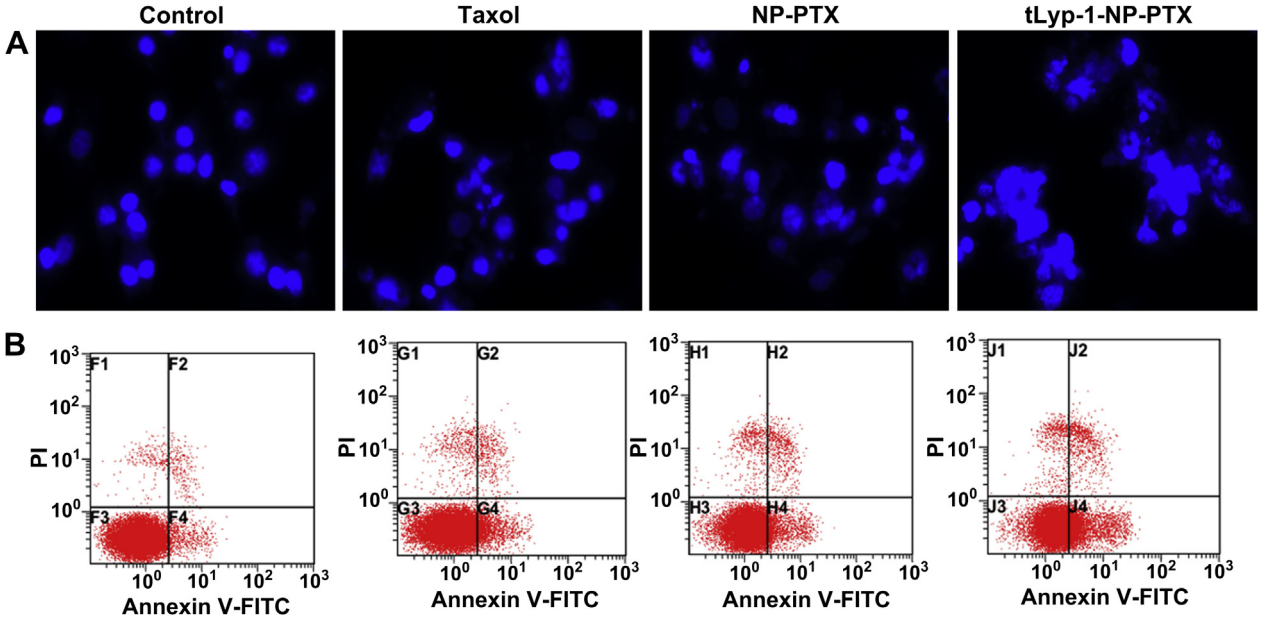

Fig. 5. Induction of apoptosis in C6 cells following 24 h incubation with various PTX formulations (PTX concentration 100 ng/ml). (A) The nuclei of C6 cells was stained with Hoechst 33258. (B) Flow cytometry analysis of apoptosis. The cells were stained with Annexin V-FITC and PI. C6 glioma cells incubated with drug-free DMEM served as the control. Original magnification: ×20.

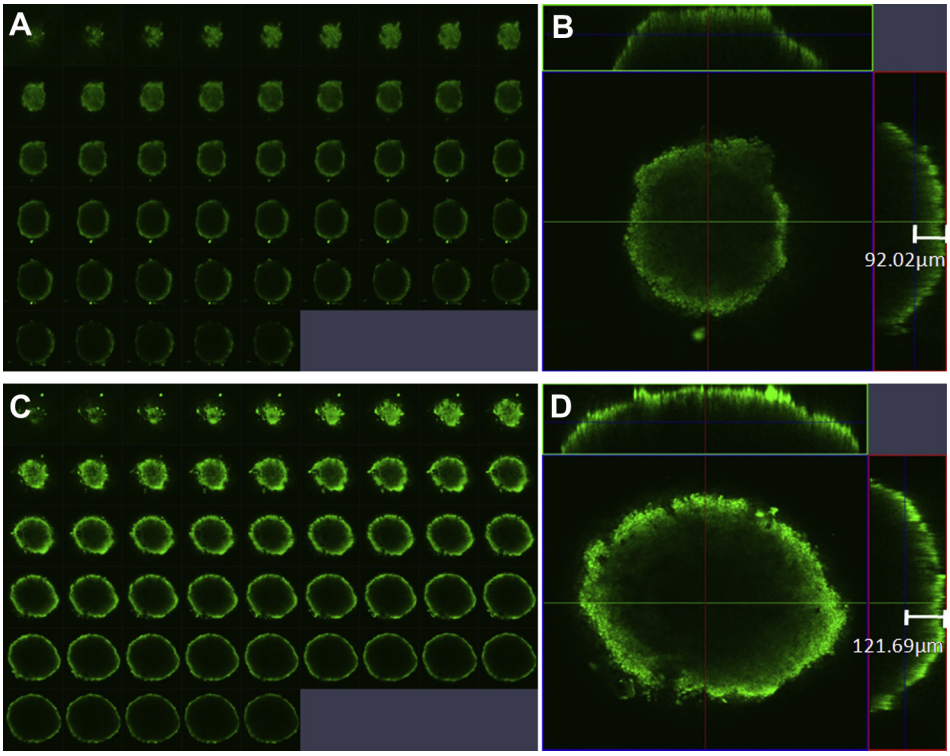

Fig. 7. Penetration of coumarin-6-labeled NP and tLyp-1-NP in avascular C6 glioma spheroids. Multi-level scan started at the top of the spheroid in 5 μm intervals of the penetration of NP (A) and tLyp-1-NP (C). Quantitative analysis of the penetration depth of NP (B) and tLyp-1-NP (D).

3.5. *In vivo experiments*

3.5.1. *In vivo imaging*

The glioma-targeting efficiency of NP and tLyp-1-NP was also investigated in nude mice bearing intracranial C6 glioma. Non-invasive NIR fluorescence imaging showed that much stronger fluorescence intensity of tLyp-1-NP was observed in the glioma site than that of NP at all the time points from 2 to 24 h following administration (Fig. 9A and B). This result was confirmed by imaging those brains collected from mice bearing intracranial glioma 24 h post-injection (Fig. 9C).

3.5.2. *Glioma distribution*

In vivo glioma permeation and targeting capability of tLyp-1-NP were studied by confocal microscopy analysis. As shown in Fig. 10, only a low accumulation of NP was observed in the glioma site and mostly at the edge of the glioma (Fig. 10A). But in the case of tLyp-1-NP, an obvious stronger fluorescent signal was detected and much deeper permeation was observed at the glioma foci (Fig. 10B).

3.5.3. *Anti-glioma effect*

The anti-glioma effect was evaluated by measuring the survival time of mice bearing intracranial C6 glioma following the treatment with different PTX formulations every three days for two weeks. As shown in Fig. 11, the medium survival time for mice treated with saline, Taxol®, NP-PTX and tLyp-1-NP-PTX was 18, 23, 28, 37 days, respectively. tLyp-1-NP-PTX significantly prolonged animal survival time when compared with NP-PTX ($^{**}p < 0.01$), Taxol® ($^{***}p < 0.001$) and saline ($^{***}p < 0.001$).

4. Discussion

Glioblastoma multiforme (GBM), the most malignant and most frequent primary brain tumor, is currently incurable, with a median survival of less than 2 years after diagnosis and treatment [29,30]. Even after gross total resection, glioma often recurs because of infiltration outside the main mass. Although chemotherapy has been demonstrated to provide a supplementary treatment after surgery, the application is largely limited by the issue of inadequate drug delivery [31,32]. Nanobiotechnology, especially nanoparticles, has made a significant contribution in chemotherapeutics for glioma by enabling passage of anti-tumor drugs across the physiological barrier and targeted therapy [33,34]. Active targeting nanoparticulate delivery system has achieved great development and provides hope for GBM therapy in recent years, in which the specificity and affinity of ligands to their receptors are crucial [35,36].

In this contribution, we utilized tLyp-1 peptide as the targeting ligand to functionalize a PEG–PLA nanoparticulate DDS for tumor angiogenic vessels and glioma cells dual-targeting drug delivery. tLyp-1 peptide, which can specifically bind to neuropilin that overexpressed on the surface of both glioma cells and endothelial cells of angiogenic blood vessels, contains a cryptic CendR motif to facilitate the nanoparticulate DDS to extravasate from tumor blood vessels and accumulate at glioma foci [37,38]. It was speculated that this tLyp-1–neuropilin interaction could mediate tumor homing, vascular extravasation and deep intra-tumor penetration of PEG–PLA nanoparticulate DDS for enhancing anti-glioma therapy.

In order to meet the demand of drug delivery into glioma, the size of nanoparticulate DDS need to be well controlled below 150 nm [39]. In this study, PEG–PLA nanoparticles were prepared through an emulsion/evaporation method, and tLyp-1 peptide was functionalized to nanoparticles via a maleimide-thiol coupling reaction. After conjugation, the size of tLyp-1-NP was found slightly increase (111.30 ± 15.64) with an average narrow distribution (0.140 ± 0.08). The sizes of NP and tLyp-1-NP were regarded as favorable for brain delivery via both enhanced permeability and retention (EPR) effect and receptor-mediated transcytosis. The

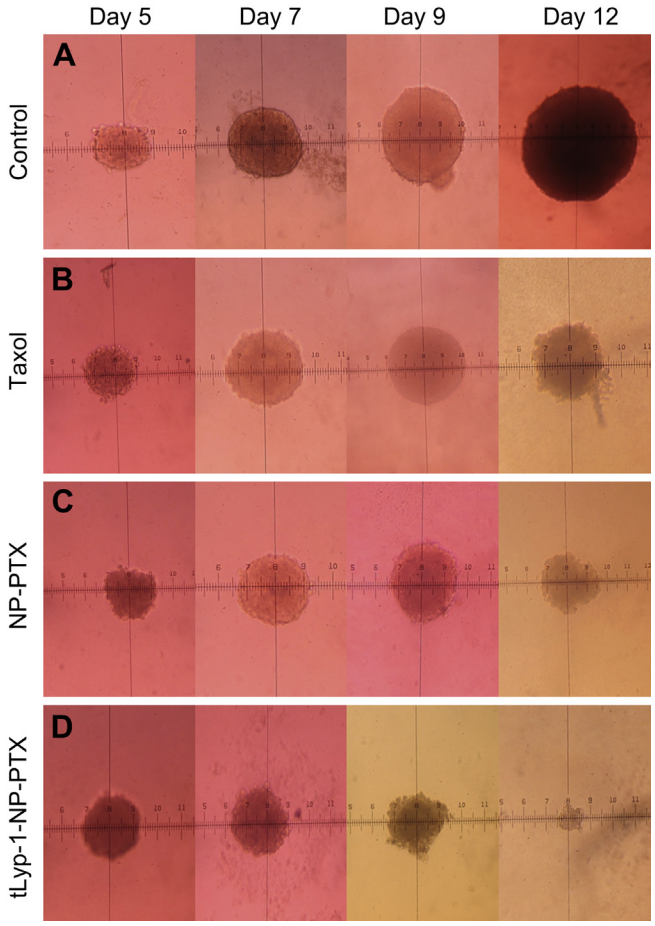

Fig. 8. Morphology of avascular C6 glioma spheroids treated with serum-free DMEM (A), Taxol® (B), NP-PTX (C) and tLyp-1-NP-PTX (D) on day 5, day 7, day 9 and day 12, respectively, at the PTX concentrations 500 ng/ml.

existence of tLyp-1 peptide on the surface of tLyp-1-NP was verified by XPS analysis with 0.53% nitrogen detected, while that on the surface of NP was undetectable (the instrumental detection limit is 0.1%). The N signal detected in the tLyp-1-NP sample was therefore believed to be attributed to tLyp-1 peptide on the nanoparticles surface.

In vitro PTX release was evaluated in PBS (pH 7.4) and PBS (pH 7.4) containing 10% rat plasma. NP-PTX and tLyp-1-NP-PTX showed almost the same biphases release pattern in both media with that in PBS (pH 7.4) slower than that in PBS (pH 7.4) containing 10% rat plasma. It was speculated that the lipase in plasma could accelerate the degradation of the polymer nanoparticles.

As the over-expressions of NRP had been note on the surface of endothelial cells of tumor angiogenic blood vessels and glioma cells, the nanoparticulate DDS functionalized with the ligand of NRP–tLyp-1 peptide would achieve a significant uptake on both endothelial cells and glioma cells. To verify this hypothesis, HUVEC and C6 glioma cells were selected as the model cells to conduct the cellular association experiments. As shown in Fig. 3, cellular association of PEG–PLA nanoparticles in both HUVEC cells and C6 glioma cells was significantly enhanced following surface conjugation with tLyp-1 peptide qualitatively and quantitatively, indicating that tLyp-1 peptide functionalization can effectively facilitate the uptake of NP in both endothelial cells of tumor angiogenic blood vessels and glioma cells. This high accumulation of tLyp-1-NP in C6 cells resulted in much stronger PTX-induced cell apoptosis and anti-proliferative effect when compared with unmodified NP. Nuclei segmentation and fragmentation was observed in C6 cells treated with PTX-loaded tLyp-1-NP after incubation for 24 h (Fig. 5A). Quantitative results from flow cytometry analysis were in good consistent with the observed results of cellular nucleus staining, indicating that tLyp-1-NP-PTX might induce more early and late apoptosis due to the high accumulation of PTX in C6 cells via a tLyp-1 peptide-mediated endocytosis. The enhanced intracellular drug delivery following tLyp-1 peptide conjugation was further confirmed by anti-proliferation assay, which showed that in C6 cells, the IC50 value of tLyp-1-NP-PTX was 2.53 folds, 3.56 folds lower than that of NP-PTX and Taxol®, respectively.

In order to elucidate the mechanism of cellular internalization of tLyp-1-NP, the effects of different endocytosis inhibitors on cellular uptake were evaluated quantitatively in both HUVEC cells and C6 glioma cells. As shown in Fig. 4A, the uptake of tLyp-1-NP in HUVEC cells was significantly inhibited by Golgi apparatus destroyer – BFA, caveolae-mediated endocytosis pathway inhibitor – filipin, lysosome inhibitor – monensin, lipid raft inhibitor – M-β-CD, microtubules depolymerization agent – nocodazole, and energy-depletion agent – NaN_3 + dg. The quantitative results indicated that the cellular uptake of tLyp-1-NP in HUVEC cells was an energy-dependent, cell skeleton-involved, and lipid raft/caveolae-mediated endocytosis with the involvement of both Golgi apparatus and lysosome. In the case of C6 cells, the uptake of tLyp-1-NP was inhibited by NaN_3 + dg and cyto-D, suggesting the participation of energy-dependent macropinocytosis pathway. In the meanwhile, the incubation with BFA and M-β-CD significantly reduced the uptake of tLyp-1-NP, indicating that the endocytosis process in C6 cells was lipid raft-mediated and Golgi apparatus involved. In addition, cellular internalization of tLyp-1-NP in both HUVEC and C6 cells was inhibited by pre-addition of tLyp-1 peptide, confirming the contribution of tLyp-1 modification to enhanced cellular uptake.

Experiments performed on monolayer tumor cells often resulted in excessively positive results because these conditions are quite different from the micro-circumstance found in solid tumors [40,41]. Therefore, 3D tumor spheroids were prepared to mimic physiologic barriers in solid tumors (heterogeneous tumor perfusion, high cell density, acidic pH and increased interstitial pressure) [42,43]. Here we exploited avascular C6 glioma spheroids to study the penetration ability of tLyp-1-NP. As shown in Fig. 7, coumarin-6-labeled tLyp-1-NP penetrated into C6 spheroids with a depth of 121.69 μm, 1.32 folds deeper than that of unmodified NP (92.02 μm), suggesting tLyp-1 peptide-functionalized nanoparticulate DDS possessed an excellent ability to penetrate deeper into the inner of solid tumor. The effect of efficient transport of tLyp-1-NP was also confirmed by the growth inhibition experiment, in which C6 spheroids treated with tLyp-1-NP-PTX exhibited the smallest volume compared with those treated with NP-PTX and Taxol®. The penetrating capability of tLyp-1-NP provide a promising approach to enhance the amount of drug accessing the inside of the solid tumors and prevent the recurrence of cancer due to the "blind areas" of chemotherapy [44,45].

In vivo near-infrared (NIR) imaging experiments were performed to further evaluate the glioma-targeting effects of tLyp-1-NP in nude mice bearing intracranial C6 glioma. As shown in Fig. 9, time-dependent accumulation of the nanoparticles at the glioma foci was observed in the mice treated with NP and tLyp-1-NP, respectively. The maximum localization of NP at glioma region was achieved at 12 h post-injection, then decreased at 24 h, indicating that the accumulation of NP at glioma site was mainly contributed by EPR effect. Compared with unmodified NP, tLyp-1-NP exhibited a significant superiority in glioma targeting with higher fluorescent intensity at all time points, indicating that the tLyp-1-mediated accumulation make a significant contribution

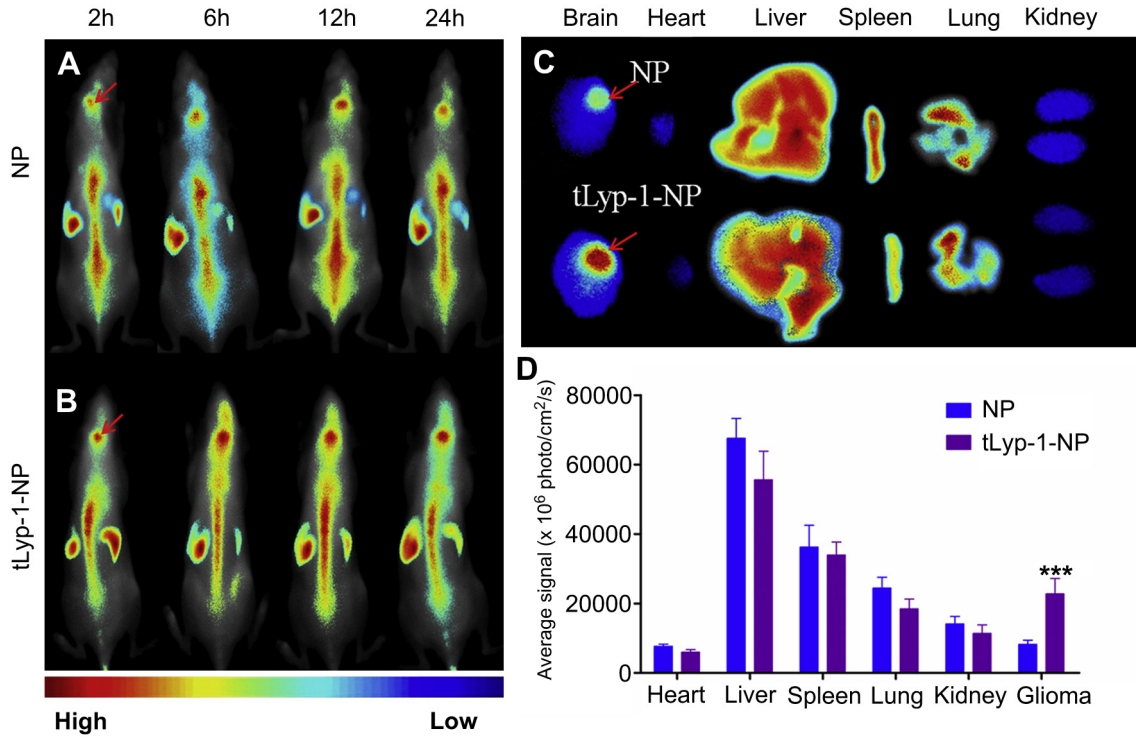

Fig. 9. In vivo near-infrared imaging of mice bearing intracranial C6 glioma intravenously treated with 200 μl DiR-labeled NP (A) and tLyp-1-NP (B) through the tail vein at 2 h, 6 h, 12 h, 24 h, respectively. In vivo fluorescence imaging of dissected organs after 24 h post-injection (C). Semi-quantitative analysis of the fluorescent intensity of the formulations in different organs and glioma (D). All the red arrows represented the site of glioma. Data represented mean ± SD ($n = 3$). $^{*}p < 0.05$, $^{**}p < 0.01$, $^{***}p < 0.001$ significantly different with that of NP group.(For interpretation of the references to colour in this figure legend, the reader is referred to the web version of this article.)

beyond EPR effect. Imaging the isolated organs showed that much stronger fluorescent intensity and more extensive distribution of tLyp-1-NP at the glioma foci, further verifying the targeting efficiency of tLyp-1-NP.

In order to intuitively evaluate the permeation and targeting efficiency of tLyp-1-NP, the frozen sections of glioma were observed under a laser scanning confocal microscopy. In consistent with the in vivo imaging experiment, it was demonstrated that a low accumulation of NP was achieved and mainly located at the edge of glioma section (Fig. 10A), suggesting EPR effect help unmodified NP reach the glioma site with only limited penetration [46,47]. In contrast, tLyp-1-NP showed a more extensive distribution and deeper penetration selectively in glioma parenchyma compared with NP. It was believed that the enhanced permeation and enrichment of tLyp-1-NP was largely contributed by the specifically overexpressed NRP receptor on the surface of both glioma cells and endothelial cells of angiogenic blood vessels as well as the CendR motif containing in tLyp-1 peptide. The C-terminal R/KXXR/K motif can specifically bind to NRP-1 receptor (a member of the neuropilin family), inducing extravasation from tumor blood vessels and facilitating penetration into tumor parenchyma [38,48].

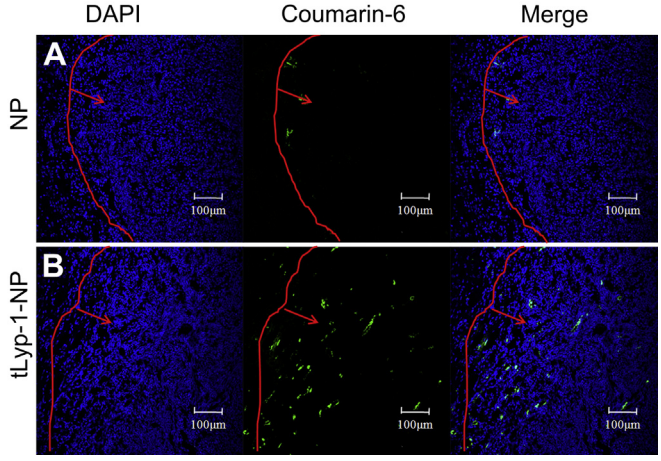

Fig. 10. In vivo glioma distribution of coumarin-6-labeled NP (A) and tLyp-1-NP (B) 3 h after administration. Blue: DAPI stained cell nuclei. Green: Coumarin-6-labeled nanoparticles. Red lines: border of the glioma. All the red arrows represented the site of glioma.(For interpretation of the references to colour in this figure legend, the reader is referred to the web version of this article.)

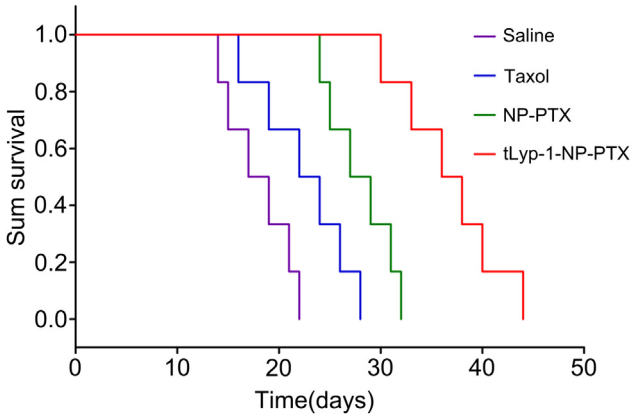

Fig. 11. Kaplan–Meier survival curve of mice bearing intracranial C6 glioma treated with saline, Taxol®, NP-PTX and tLyp-1-NP-PTX every three days in two weeks at PTX dose of 5 mg/kg ($n = 6$).

The improved accumulation and penetration of tLyp-1-NP-PTX at the glioma foci led to an anticipated enhanced anti-glioma efficacy in vivo. As shown in Kaplan–Meier survival curve (Fig. 11), an enormous prolonged survival (the medium survival time 37 days) was achieved in those mice bearing intracranial C6 glioma treated with tLyp-1-NP-PTX, significantly higher than that of those treated with NP-PTX (28 days, $^{**}p < 0.01$), Taxol® (23 days, $^{***}p < 0.001$) and saline (18 days, $^{***}p < 0.001$).

5. Conclusion

We here developed a nanoparticulate DDS decorated with a tumor homing and penetrating peptide, tLyp-1 peptide, as the dual-targeting ligand for anti-glioma drug delivery. The tLyp-1 peptide was conjugated to the surface of PEG–PLA nanoparticles via a maleimide-thiol coupling reaction. The resulted tLyp-1-NP showed uniformly spherical in shape under TEM with particle size of 111.30 ± 15.64 nm and the peptide conjugation confirmed by XPS analysis. Enhanced cellular uptake of tLyp-1-NP was achieved in both HUVEC cells and C6 cells, which thus achieved improved cytotoxicity of the payload – PTX. More importantly, improved tumor-selective accumulation and penetration of tLyp-1-NP was observed in both avascular C6 glioma spheroids and mice bearing intracranial C6 glioma. Due to these optimal biopharmaceutical properties, tLyp-1-NP-PTX treatment achieved the longest survival in mice bearing intracranial C6 glioma. Taken these results together, we claimed tLyp-1 peptide-functionalized PEG–PLA nanoparticulate DDS might serve as an effective nanocarrier for anti-glioma drug delivery.

Acknowledgments

This work was supported by National Key Basic Research Program (2013CB932502), National Natural Science Foundation of China (81072592), National Science and Technology major Project (2012ZX09304004), Innovation Program of Shanghai Municipal Education Commission (12ZZ107), Program for New Century Excellent Talents in University and Grants from Shanghai Science and Technology Committee (11430702200, 12ZR1416300 and 12nm0502000). The authors also acknowledge the support from School of Pharmacy, Fudan University & the Open Project Program of Key Lab of Smart Drug Delivery (Fudan University), Ministry of Education & PLA, China (2011SDD-10).

References

[1] Jain KK. Use of nanoparticles for drug delivery in glioblastoma multiforme. Expert Rev Neurother 2007;7:363–72.
[2] Behin A, Hoang-Xuan K, Carpentier AF, Delattre JY. Primary brain tumours in adults. Lancet 2003;361:323–31.
[3] Wen PY, Kesari S. Malignant gliomas in adults. N Engl J Med 2008;359:492–507.
[4] Newton HB. Advances in strategies to improve drug delivery to brain tumors. Expert Rev Neurother 2006;6:1495–509.
[5] Groothuis DR. The blood-brain and blood-tumor barriers: a review of strategies for increasing drug delivery. Neuro Oncol 2000;2:45–59.
[6] Liu Y, Lu W. Recent advances in brain tumor-targeted nano-drug delivery systems. Expert Opin Drug Deliv 2012;9:671–86.
[7] Beduneau A, Saulnier P, Benoit JP. Active targeting of brain tumors using nanocarriers. Biomaterials 2007;28:4947–67.
[8] Cheng Z, Al Zaki A, Hui JZ, Muzykantov VR, Tsourkas A. Multifunctional nanoparticles: cost versus benefit of adding targeting and imaging capabilities. Science 2012;338:903–10.
[9] Meyers JD, Doane T, Burda C, Basilion JP. Nanoparticles for imaging and treating brain cancer. Nanomedicine (Lond) 2013;8:123–43.
[10] Nicolas J, Mura S, Brambilla D, Mackiewicz N, Couvreur P. Design, functionalization strategies and biomedical applications of targeted biodegradable/biocompatible polymer-based nanocarriers for drug delivery. Chem Soc Rev 2013;42:1147–235.
[11] Pang Z, Feng L, Hua R, Chen J, Gao H, Pan S, et al. Lactoferrin-conjugated biodegradable polymersome holding doxorubicin and tetrandrine for chemotherapy of glioma rats. Mol Pharm 2010;7:1995–2005.
[12] Gu G, Xia H, Hu Q, Liu Z, Jiang M, Kang T, et al. PEG-co-PCL nanoparticles modified with MMP-2/9 activatable low molecular weight protamine for enhanced targeted glioblastoma therapy. Biomaterials 2013;34:196–208.
[13] He H, Li Y, Jia XR, Du J, Ying X, Lu WL, et al. PEGylated poly(amidoamine) dendrimer-based dual-targeting carrier for treating brain tumors. Biomaterials 2011;32:478–87.
[14] Xin H, Jiang X, Gu J, Sha X, Chen L, Law K, et al. Angiopep-conjugated poly(ethylene glycol)-co-poly(epsilon-caprolactone) nanoparticles as dual-targeting drug delivery system for brain glioma. Biomaterials 2011;32:4293–305.
[15] Plate KH, Scholz A, Dumont DJ. Tumor angiogenesis and anti-angiogenic therapy in malignant gliomas revisited. Acta Neuropathol 2012;124:763–75.
[16] Soffietti R, Trevisan E, Bertero L, Bosa C, Ruda R. Anti-angiogenic approaches to malignant gliomas. Curr Cancer Drug Targets 2012;12:279–88.
[17] Paez-Ribes M, Allen E, Hudock J, Takeda T, Okuyama H, Vinals F, et al. Anti-angiogenic therapy elicits malignant progression of tumors to increased local invasion and distant metastasis. Cancer Cell 2009;15:220–31.
[18] Nasarre C, Roth M, Jacob L, Roth L, Koncina E, Thien A, et al. Peptide-based interference of the transmembrane domain of neuropilin-1 inhibits glioma growth in vivo. Oncogene 2010;29:2381–92.
[19] Li P, Rossman TG. Genes upregulated in lead-resistant glioma cells reveal possible targets for lead-induced developmental neurotoxicity. Toxicol Sci 2001;64:90–9.
[20] He Z, Tessier-Lavigne M. Neuropilin is a receptor for the axonal chemorepellent Semaphorin III. Cell. 1997;90:739–51.
[21] Rizzolio S, Tamagnone L. Multifaceted role of neuropilins in cancer. Curr Med Chem 2011;18:3563–75.
[22] Roth L, Agemy L, Kotamraju VR, Braun G, Teesalu T, Sugahara KN, et al. Transtumoral targeting enabled by a novel neuropilin-binding peptide. Oncogene 2012;31:3754–63.
[23] Sugahara KN, Teesalu T, Karmali PP, Kotamraju VR, Agemy L, Girard OM, et al. Tissue-penetrating delivery of compounds and nanoparticles into tumors. Cancer Cell 2009;16:510–20.
[24] Xia H, Gao X, Gu G, Liu Z, Zeng N, Hu Q, et al. Low molecular weight protamine-functionalized nanoparticles for drug delivery to the brain after intranasal administration. Biomaterials 2011;32:9888–98.
[25] Xia H, Gao X, Gu G, Liu Z, Hu Q, Tu Y, et al. Penetratin-functionalized PEG-PLA nanoparticles for brain drug delivery. Int J Pharm 2012;436:840–50.
[26] Zeng N, Hu Q, Liu Z, Gao X, Hu R, Song Q, et al. Preparation and characterization of paclitaxel-loaded DSPE-PEG-liquid crystalline nanoparticles (LCNPs) for improved bioavailability. Int J Pharm 2012;424:58–66.
[27] Zeng N, Gao X, Hu Q, Song Q, Xia H, Liu Z, et al. Lipid-based liquid crystalline nanoparticles as oral drug delivery vehicles for poorly water-soluble drugs: cellular interaction and in vivo absorption. Int J Nanomed 2012;7:3703–18.
[28] Jiang X, Xin H, Gu J, Xu X, Xia W, Chen S, et al. Solid tumor penetration by integrin-mediated pegylated poly(trimethylene carbonate) nanoparticles loaded with paclitaxel. Biomaterials 2013;34:1739–46.
[29] Tanaka S, Louis DN, Curry WT, Batchelor TT, Dietrich J. Diagnostic and therapeutic avenues for glioblastoma: no longer a dead end? Nat Rev Clin Oncol 2012;10:14–26.
[30] Huse JT, Holland E, Deangelis LM. Glioblastoma: molecular analysis and clinical implications. Annu Rev Med 2013;64:59–70.
[31] Stewart LA. Chemotherapy in adult high-grade glioma: a systematic review and meta-analysis of individual patient data from 12 randomised trials. Lancet 2002;359:1011–8.
[32] Eramo A, Ricci-Vitiani L, Zeuner A, Pallini R, Lotti F, Sette G, et al. Chemotherapy resistance of glioblastoma stem cells. Cell Death Differ 2006;13:1238–41.
[33] Yang H. Nanoparticle-mediated brain-specific drug delivery, imaging, and diagnosis. Pharm Res 2010;27:1759–71.
[34] Roger M, Clavreul A, Venier-Julienne MC, Passirani C, Montero-Menei C, Menei P. The potential of combinations of drug-loaded nanoparticle systems and adult stem cells for glioma therapy. Biomaterials 2011;32:2106–16.
[35] Gao H, Qian J, Yang Z, Pang Z, Xi Z, Cao S, et al. Whole-cell SELEX aptamer-functionalised poly(ethyleneglycol)-poly(epsilon-caprolactone) nanoparticles for enhanced targeted glioblastoma therapy. Biomaterials 2012;33:6264–72.
[36] Jiang X, Sha X, Xin H, Chen L, Gao X, Wang X, et al. Self-aggregated pegylated poly (trimethylene carbonate) nanoparticles decorated with c(RGDyK) peptide for targeted paclitaxel delivery to integrin-rich tumors. Biomaterials 2011;32:9457–69.
[37] Sugahara KN, Teesalu T, Karmali PP, Kotamraju VR, Agemy L, Greenwald DR, et al. Coadministration of a tumor-penetrating peptide enhances the efficacy of cancer drugs. Science 2010;328:1031–5.
[38] Ruoslahti E. Peptides as targeting elements and tissue penetration devices for nanoparticles. Adv Mater 2012;24:3747–56.
[39] Agemy L, Friedmann-Morvinski D, Kotamraju VR, Roth L, Sugahara KN, Girard OM, et al. Targeted nanoparticle enhanced proapoptotic peptide as potential therapy for glioblastoma. Proc Natl Acad Sci USA 2011;108:17450–5.
[40] Minchinton AI, Tannock IF. Drug penetration in solid tumours. Nat Rev Cancer 2006;6:583–92.

[41] Cairns R, Papandreou I, Denko N. Overcoming physiologic barriers to cancer treatment by molecularly targeting the tumor microenvironment. Mol Cancer Res 2006;4:61–70.
[42] Shirinifard A, Gens JS, Zaitlen BL, Poplawski NJ, Swat M, Glazier JA. 3D multi-cell simulation of tumor growth and angiogenesis. PLoS One 2009;4:e7190.
[43] Hirschhaeuser F, Menne H, Dittfeld C, West J, Mueller-Klieser W, Kunz-Schughart LA. Multicellular tumor spheroids: an underestimated tool is catching up again. J Biotechnol 2010;148:3–15.
[44] Chauhan VP, Stylianopoulos T, Boucher Y, Jain RK. Delivery of molecular and nanoscale medicine to tumors: transport barriers and strategies. Annu Rev Chem Biomol Eng 2011;2:281–98.
[45] Jain RK. Delivery of molecular and cellular medicine to solid tumors. Adv Drug Deliv Rev 2001;46:149–68.
[46] Fang J, Nakamura H, Maeda H. The EPR effect: unique features of tumor blood vessels for drug delivery, factors involved, and limitations and augmentation of the effect. Adv Drug Deliv Rev 2011;63:136–51.
[47] Maeda H, Wu J, Sawa T, Matsumura Y, Hori K. Tumor vascular permeability and the EPR effect in macromolecular therapeutics: a review. J Control Release 2000;65:271–84.
[48] Hu Q, Gu G, Liu Z, Jiang M, Kang T, Miao D, et al. F3 peptide-functionalized PEG-PLA nanoparticles co-administrated with tLyp-1 peptide for anti-glioma drug delivery. Biomaterials 2013;34:1135–45.